Optimal Shape Control of Composite Thin Plates with Piezoelectric Actuators

Daqun Tong and Robert L. Williams II
Department of Mechanical Engineering
Ohio University
Athens, Ohio

Sunil K. Agrawal
Department of Mechanical Engineering
University of Delaware
Newark, Delaware

Journal of Intelligent Material Systems and Structures
Vol. 9, pp. 458-467
June, 1998

Corresponding author information:
Robert L. Williams II
Assistant Professor
Department of Mechanical Engineering
257 Stocker Center
Ohio University
Athens, OH 45701-2979
phone: (740) 593-1096
fax: (740) 593-0476
email: bobw@bobcat.ent.ohiou.edu
URL: http://www.ent.ohiou.edu/~bobw

Optimal Shape Control of Composite Thin Plates with Piezoelectric Actuators

Daqun Tong[1] and Robert L. Williams II[2]
Department of Mechanical Engineering
Ohio University
Athens, Ohio

Sunil K. Agrawal[3]
Department of Mechanical Engineering
University of Delaware
Newark, Delaware

KEYWORDS: Piezoelectric actuators, Composite thin plate, optimal shape control

ABSTRACT

Emerging technologies in microsensing, microactuation, active airfoils, turbine blades, and large, lightweight, flexible space structures can benefit from piezoelectric actuators for active shape control. Piezoelectric materials develop strain under applied voltage which induces structural deflection. This article presents analytical models, FEM solution, and optimal shape control of composite thin plates with piezoelectric actuators surface embedded or bonded in a biomorph arrangement. A 2D FEM approach is developed which is accurate, plus simpler and more efficient than existing 3D solutions. Three optimal shape problems are presented: applied voltage, actuator layout, and actuator number optimizations. For the latter two problems, a novel method is introduced using a vector of binary variables.

[1] Graduate Research Assistant
[2] Assistant Professor, Corresponding Author
[3] Associate Professor

INTRODUCTION

The integration of composite materials with piezoelectric actuators will significantly improve the performance of aircraft and space structures. The feasibility of such integrated smart structures has been demonstrated by various analyses and numerical models (e.g. Donthireddy and Chandrashekhara, 1996; Ghosh and Batra, 1995; Crawley and Lazarus, 1991; Lee and Moon, 1990). An overview of smart structure technology is presented by Gandhi and Thompson (1992); few problems have extended to practical designs (Jia and Rogers, 1989; Sepulveda and Schmit, 1991).

Shape optimization for such structures is of great importance, especially in low-weight aerospace applications. The effectiveness of the control system strongly depends on the active element locations (Fanson and Caughey, 1987). In those 3D models, the problems are large and complex. For example, a plate with thin sensors and actuators is modeled with the isoparametric hexahedron solid element (Sepulveda and Schmit, 1991), requiring Guyan reduction to reduce the total degrees of freedom (dof). When the plate is very thin, there are problems of excessive shear strain energies and higher stiffness coefficients in the thickness direction. Another example is applying an 8-node, 32-dof brick element to a thin plate example (Sepulveda and Schmidt, 1991); 3D incompatible modes were necessary for predicting the deflection.

Presented in a previous article (Agrawal, Tong, and Nagaraja, 1994) is a 1D model, finite difference solution, and optimal input voltage estimation for a cantilevered composite beam. The current article extends this work to formal optimization problems for a thin plate, while maintaining computational efficiency for practical application. This article is organized as follows. First, a simpler (relative to existing 3D models) 2D mathematical model for the deflection of a composite thin plate with piezoelectric actuators surface embedded or bonded is presented. Then an efficient FEM solution is presented using a 4-node, 12-dof thin plate discrete Kirchhoff quadrilateral (DKQ) bending element. Shape optimization is then developed, for the optimal input voltages, optimal actuators layout, and optimal number of actuators problems. These optimization problems may be used either off-line for optimal design or for real-time shape control. Last, two examples are given.

MATHEMATICAL MODELS OF COMPOSITE THIN PLATE

System Description and Assumptions

The actuator/plate system is a homogeneous, elastic, anisotropic (we also consider isotropic) laminated composite thin plate. Piezoelectric actuators are embedded or bonded on its top and bottom surfaces in a bimorph arrangement (for every actuator on the top, another exists in the same location on the bottom). The piezoelectric actuators are modeled as homogeneous, elastic, and transversely isotropic in mechanical and piezoelectric behavior. In Figure 1, angle θ aligns x_1 parallel to the fibers while x_2 is normal to the fibers.

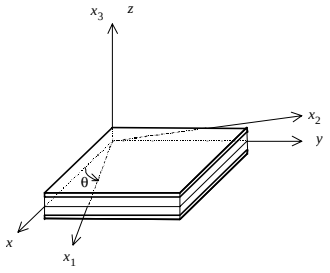

Figure 1. Composite Thin Plate Geometry

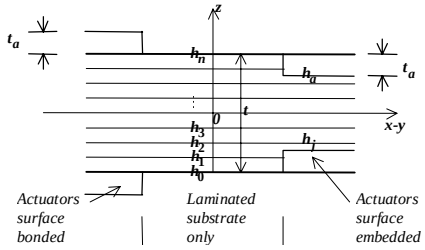

Figure 2. Cross-Section of Thin Plate

The substrate cross section is shown in Figure 2. The actuator and substrate plates are given the subscripts *a* and *s* respectively. The actuator plate thickness is t_a and the total thickness of the plate is t. The poling direction of all actuator plates is the z axis. The applied electric fields on the top and bottom actuators of each bimorph have the same electric potential. One is in the poling direction and the second is opposite, thus inducing extension in one actuator and contraction in the other. Such pairing is favorable for Kirchhoff's assumptions (Ugrual, 1981) which are used for model simplification. Perfect actuator bonding is assumed (deformations in the actuators and substrates at a point on a bonding surface are equal). The interlaminar bonding layer between the actuators and substrates is sufficiently thin that neglecting the shear layer will not introduce any significant errors into the model (Crawley and Lazarus, 1991).

***U-V-W* Model**

This section summarizes the *U-V-W* composite thin plate model (*U-V-W* are the *X,Y,Z,* displacements of a point on the thin plate mid-plane). Equations (1-3) present the mathematical model; for detailed derivation see Tong (1997). It was derived as follows. For a differential plate element of dimension *dx*, *dy*, *dz*, located at point (*x*, *y*, *z*), the kinematic strain-displacement relationships, stress-strain relationship, stress resultant, stress couples, and shear resultants were written. The general anisotropic case was considered, both for locations with and without actuators surface embedded or surface bonded. Performing a force and moment balance for the differential element (neglecting the body force term for simplicity), integrating term by term across each ply, and summing across plies of the plate yielded five equilibrium equations which were combined into three independent equilibrium conditions. The relationships discussed above were substituted into the three equilibrium equations to yield:

$$A_{11}\frac{\partial^2 U}{\partial x^2}+2A_{16}\frac{\partial^2 U}{\partial x\partial y}+A_{66}\frac{\partial^2 U}{\partial y^2}+A_{16}\frac{\partial^2 V}{\partial x^2}+(A_{12}+A_{66})\frac{\partial^2 V}{\partial x\partial y}+A_{26}\frac{\partial^2 V}{\partial y^2}$$

$$-B_{11}\frac{\partial^3 W}{\partial x^3}-3B_{16}\frac{\partial^3 W}{\partial x^2\partial y}-(B_{12}+2B_{66})\frac{\partial^3 W}{\partial x\partial y^2}-B_{26}\frac{\partial^3 W}{\partial y^3}+\xi_x=0 \quad (1)$$

$$A_{16}\frac{\partial^2 U}{\partial x^2}+(A_{12}+A_{66})\frac{\partial^2 U}{\partial x\partial y}+A_{26}\frac{\partial^2 U}{\partial y^2}+A_{66}\frac{\partial^2 V}{\partial x^2}+2A_{26}\frac{\partial^2 V}{\partial x\partial y}+A_{22}\frac{\partial^2 V}{\partial y^2}$$

$$-B_{16}\frac{\partial^3 W}{\partial x^3}-(B_{12}+2B_{66})\frac{\partial^3 W}{\partial x^2\partial y}-3B_{26}\frac{\partial^3 W}{\partial x\partial y^2}-B_{22}\frac{\partial^3 W}{\partial y^3}+\xi_y=0 \quad (2)$$

$$B_{11}\frac{\partial^3 U}{\partial x^3}+3B_{16}\frac{\partial^3 U}{\partial x^2\partial y}+(B_{12}+2B_{66})\frac{\partial^3 U}{\partial x\partial y^2}+B_{26}\frac{\partial^3 U}{\partial y^3}$$

$$+B_{16}\frac{\partial^3 V}{\partial x^3}+(B_{12}+2B_{66})\frac{\partial^3 V}{\partial x^2\partial y}+3B_{26}\frac{\partial^3 V}{\partial x\partial y^2}+B_{22}\frac{\partial^3 V}{\partial y^3}$$

$$-D_{11}\frac{\partial^4 W}{\partial x^4}-4D_{16}\frac{\partial^4 W}{\partial x^3\partial y}-2(D_{12}+2D_{66})\frac{\partial^4 W}{\partial x^2\partial y^2}-4D_{26}\frac{\partial^4 W}{\partial x\partial y^3}-D_{22}\frac{\partial^4 W}{\partial y^4}+\frac{h}{2}\left(\frac{\partial\zeta_x}{\partial x}+\frac{\partial\zeta_y}{\partial y}\right)=0 \quad (3)$$

where:

$$\xi_x = \tau_{1x} - \tau_{2x} \qquad \xi_y = \tau_{1y} - \tau_{2y} \qquad \zeta_x = \tau_{1x} + \tau_{2x} \qquad \zeta_y = \tau_{1y} + \tau_{2y} \tag{4}$$

and τ_i are the surface tractions.

The voltage applied on the actuators does not appear in the governing equations explicitly because the piezoelectric actuation strain is not a function of *x*, *y* but only the input voltages.

Matrix elements A_{ij}, B_{ij} and D_{ij} are given as follows for various conditions (locations with and without actuators surface embedded or bonded, plus anisotropic or isotropic substrate). For an anisotropic laminated substrate of composite material, at a location with no actuators, *A*, *B* and *D* are:

$$A = \int_t Q dz = \sum_{k=1}^{n} \overline{Q}_{sk}(h_k - h_{k-1}) \qquad B = \int_t Q z dz = \frac{1}{2}\sum_{k=1}^{n} \overline{Q}_{sk}(h_k^2 - h_{k-1}^2)$$

$$D = \int_t Q z^2 dz = \frac{1}{3}\sum_{k=1}^{n} \overline{Q}_{sk}(h_k^3 - h_{k-1}^3) \tag{5}$$

The matrix $\overline{Q}_s$ is from the stress-strain relationship $\sigma = \overline{Q}_s \varepsilon$ (see Tong, 1997 for details). All h_i refer to heights in the laminated substrate (see Figure 2). At a location with actuators surface embedded, *A*′, *B*′ and *D*′ are:

$$A' = \sum_{k=j+1}^{n-j} \overline{Q}_{sk}(h_k - h_{k-1}) + \overline{Q}_{sj}(h_j + h_a) + \overline{Q}_{sn-j+1}(h_a - h_{n-j}) + 2Q_a t_a$$

$$B' = \frac{1}{2}\sum_{k=j+1}^{n-j} \overline{Q}_{sk}(h_k^2 - h_{k-1}^2) + \overline{Q}_{sj}(h_j^2 - h_a^2) + \overline{Q}_{sn-j+1}(h_a^2 - h_{n-j}^2)$$

$$D' = \frac{1}{3}\sum_{k=j+1}^{n-j} \overline{Q}_{sk}(h_k^3 - h_{k-1}^3) + \frac{1}{3}\overline{Q}_{sj}(h_j^3 + h_a^3) + \frac{1}{3}\overline{Q}_{sn-j+1}(h_a^3 - h_{n-j}^3) + \frac{2}{3}Q_a\left(h_n^3 - h_a^3\right) \tag{6}$$

with

$$h_a = h_n - t_a = \frac{t}{2} - t_a \tag{7}$$

where matrix Q_a is the inverse of the piezoelectric actuator stiffness matrix S_a:

$$Q_a = S_a^{-1} = \frac{E_{1a}}{1-\nu_{1a}^2}\begin{bmatrix} 1 & \nu_{1a} & 0 \\ \nu_{1a} & 1 & 0 \\ 0 & 0 & (1-\nu_{1a})/2 \end{bmatrix} \tag{8}$$

E and ν are Young's modulus and Poisson's ratio of the actuator material. The subscript 1 indicates behavior in the x-y plane, a indicates actuator, and s indicates substrate. In Equations (6), j is the layer number of the beginning substrate ply which contains no actuators (see Figure 2), and the $'$ mark is used to distinguish A, B, and D from those of no actuators. For locations where there are surface bonded actuators:

$$A' = \sum_{k=1}^{n} \overline{Q}_{sk}(h_k - h_{k-1}) + 2Q_a t_a \qquad B' = \frac{1}{2}\sum_{k=1}^{n} \overline{Q}_{sk}(h_k^2 - h_{k-1}^2)$$

$$D' = \frac{1}{3}\sum_{k=1}^{n} \overline{Q}_{sk}(h_k^3 - h_{k-1}^3) + \frac{2}{3}Q_a[(h_n + t_a)^3 - h_n^3] \tag{9}$$

For isotropic substrate material, the above matrices are simpler. Since the substrate is mid-plane symmetric, $B = 0$, and:

$$A = Q_s t \qquad D = Q_s \frac{t^3}{12} \tag{10}$$

for a location with no actuators, and:

$$A' = Q_s(t - 2t_a) + 2Q_a t_a \qquad D' = Q_s \frac{(t-2t_a)^3}{12} + Q_a \frac{t^3 - (t-2t_a)^3}{12} \tag{11}$$

for a location with actuators surface embedded. For the surface bonded case, substitute $(t–2t_a)$ for t to compute A and D, while A' and D' remain the same as Equation (11). If the substrate material is isotropic, the following definitions apply:

$$\overline{Q}_s = Q_s = \frac{E_a}{1-\nu_a^2}\begin{bmatrix} 1 & \nu_a & 0 \\ \nu_a & 1 & 0 \\ 0 & 0 & (1-\nu_a)/2 \end{bmatrix} \tag{12}$$

Φ-W Model

The U-V-W variables may be further reduced to two variables as follows. The in-plane displacements U and V are uncoupled from the normal displacement W and the in-plane shear strain γ_{0xy} is related to the normal strains ε_{0x} and ε_{0y} via U and V. The in-plane displacements U and V can be combined into the dependent variable Φ (Airy stress function, Calcote, 1969):

$$N_x = \frac{\partial^2 \Phi}{\partial y^2} - \eta_x \qquad N_y = \frac{\partial^2 \Phi}{\partial x^2} - \eta_y \qquad N_{xy} = -\frac{\partial^2 \Phi}{\partial x \partial y} \tag{13}$$

where:

$$\eta_x = \int (\tau_{1x} - \tau_{2x}) dx \qquad \eta_y = \int (\tau_{1y} - \tau_{2y}) dy \tag{14}$$

and N_i represent the stress resultants. The anisotropic Φ-W model is given in Tong (1997). For orthotropic substrate plies with mid-plane symmetry, Φ is uncoupled from W, and the two equations are:

$$a_{22}\frac{\partial^4 \Phi}{\partial x^4} - 2a_{23}\frac{\partial^4 \Phi}{\partial x^3 \partial y} + (2a_{12} + a_{33})\frac{\partial^4 \Phi}{\partial x^2 \partial y^2} - 2a_{13}\frac{\partial^4 \Phi}{\partial x \partial y^3} + a_{11}\frac{\partial^4 \Phi}{\partial y^4}$$
$$- a_{22}\frac{\partial^2 \eta_y}{\partial x^2} - a_{11}\frac{\partial^2 \eta_x}{\partial y^2} - a_{12}\left(\frac{\partial \xi_y}{\partial x} + \frac{\partial \xi_x}{\partial y}\right) + a_{23}\frac{\partial \xi_y}{\partial x} + a_{13}\frac{\partial \xi_x}{\partial y} = 0 \tag{15}$$

$$D_{11}\frac{\partial^4 W}{\partial x^4} + 4D_{16}\frac{\partial^4 W}{\partial x^3 \partial y} + 2(D_{12} + 2D_{66})\frac{\partial^4 W}{\partial x^2 \partial y^2} + 4D_{26}\frac{\partial^4 W}{\partial x \partial y^3} + D_{22}\frac{\partial^4 W}{\partial y^4} - \frac{h}{2}\left(\frac{\partial \zeta_x}{\partial x} + \frac{\partial \zeta_y}{\partial y}\right) = 0 \tag{16}$$

where $a = A^{-1}$.

Boundary Conditions

To complete the mathematical description of the plate governed by fourth-order partial differential equations, four boundary conditions are required, corresponding to constraints on each edge of the plate. For a clamped edge, pinned edge, edge on rollers, and a free edge, the boundary conditions are given in Equations (17-20), respectively.

$$\begin{aligned} U = V = W = \frac{\partial W}{\partial y} = 0 \\ U = V = W = M_y = 0 \\ N_y = N_{xy} = W = M_y = 0 \\ N_y = N_{xy} = M_y = \overline{V}_y = 0 \end{aligned} \tag{17-20}$$

where M_i represent the stress couples and $\overline{V}_i$ are the Kirchhoff effective transverse shear forces. When shape control of the plate or the response of the flexural vibration is considered, usually only normal displacement W is of interest. If in-plane displacements U, V can be ignored, only two boundary conditions are required on each edge of a plate. They can be transverse deflection and slope, or force and moment, or some combination. In the boundary conditions (Equations 17-20), if the in-plane deflection U and V and the in-plane normal forces N_x and N_y are dropped, the remaining expressions are the boundary conditions for solving normal deflection W only.

FEM SOLUTION

The governing partial differential equations (*U-V-W* model, Equations (1-3), or *Φ-W* model, Equations (15-16)), subject to specified boundary conditions, are solved in this section using the finite element method (FEM) based on the Theorem of Minimum Potential Energy. In addition to assumptions stated earlier, it is further assumed that the in-plane displacements *U* and *V* are negligible. The governing equation to solve is then Equation (16). A simple 2D FEM model for solving the normal deflection *W* using the Discrete Kirchoff Quadrilateral (DKQ) thin plate bending element is employed. This section presents the highlights of this FEM approach; for details see Tong (1997). In previous work (Agrawal, Tong, and Nagaraja, 1994) a 1D finite difference method was employed.

Element Equations

The four-node, 12-dof DKQ element is shown in Figure 3. It relates the rotations of the normal to that of the undeformed midplane, $\beta_x = -\partial W/\partial x$ and $\beta_y = -\partial W/\partial y$, such that: (a) the nodal variables are the transverse displacement *W* and its derivatives at the four corner nodes, $\theta_x = W_{,y}$ and $\theta_y = -W_{,x}$ (where $(\bullet)_{,x}$ represents $\partial(\bullet)/\partial x$); and (b) the Kirchoff assumptions are satisfied along the boundary of the element. The twelve DKQ nodal variables are $q^e = \{\cdots \quad W_i \quad \theta_{xi} \quad \theta_{yi} \quad \cdots\}^T$, i=1,2,3,4. The rotations are $\beta_x = H^x(\xi,\eta)q^e$ and $\beta_y = H^y(\xi,\eta)q^e$ where $H^x(\xi,\eta)$ and $H^y(\xi,\eta)$ are interpolation functions for β_x and β_y, respectively, with 12 elements each (given in Tong, 1997).

Following standard finite element procedures (e.g. Hughes, 1987), the equilibrium equations (minimizing the potential energy of each element) are expressed in terms of the nodal displacements:

$$K^e q^e = F^e \tag{21}$$

where $K^e = \int_{\Gamma^e} B^T D B d\Gamma$ is the element stiffness matrix and $F^e = F^e_{Tr} + F^e_T + F^e_V$ is the force vector, where F^e_{Tr}, F^e_T and F^e_V are the element surface traction force, thermal force, and piezoelectric actuation force. F^e_V

is zero for elements with no actuators. The element stiffness matrix and force vectors are calculated by using 2×2 Gauss numerical integration:

$$K^e = \int_{-1}^{+1}\int_{-1}^{+1} B^T D B \left|J\right| d\xi d\eta \qquad F_{Tr}^e = \int_{-1}^{+1}\int_{-1}^{+1} B^T \bar{t} \left|J\right| d\xi d\eta$$

$$F_T^e = \int_{-1}^{+1}\int_{-1}^{+1} B^T M_T \left|J\right| d\xi d\eta \qquad F_V^e = \int_{-1}^{+1}\int_{-1}^{+1} B^T M_\lambda \left|J\right| d\xi d\eta \tag{22}$$

where J is the Jacobian matrix of the transformation between the parent and actual elements, B is the matrix mapping nodal variables into the mid-plane curvature vector, D is from the modeling section, M is the stress couple, M_λ is the bending moment from piezoelectric actuation, and $\bar{t}$ is the given surface traction coefficient (all of these details are given in Tong, 1997). Since matrix B is 3×12, the element stiffness matrix K^e is 12×12; it is also symmetric.

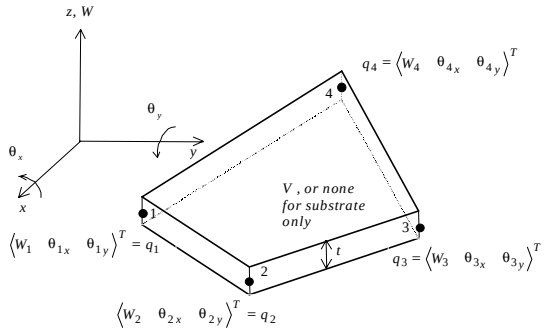

Figure 3. 12-dof DKQ Plate Bending Element

System Equations

The global system equation is expressed as

$$Kq = F \tag{23}$$

where K and F are the global stiffness matrix and force vector, determined through standard FEM procedures. A mapping matrix P^e is formed for each element, relating the contribution of each element stiffness matrix to the global stiffness matrix. The global stiffness matrix and global force vector are assembled as:

$$K = \sum_{i=1}^{n_e} (P_i^e)^T K_i^e P_i^e \qquad F = \sum_{i=1}^{n_e} (P_i^e)^T F_i^e = \sum_{j=1}^{n_e} (P_i^e)^T (F_{Tr\,i}^e + F_{T\,j}^e + F_{V\,i}^e) \qquad (24\text{-}25)$$

Comparison of 2D and 3D Solutions

To test the validity of the proposed 2D DKQ FEM solution, two actuator/plate systems were simulated. These were cantilevered laminated composite thin plates with 15 piezoelectric actuators bonded to each surface in a bimorph arrangement. The two substrates (whose stacking sequences are $[0/\pm45]_s$ and $[+30_2/0]_s$) were constructed from Hercules AS4/3501 Graphite/Epoxy and were designed for the laminate composite substrates to increase transverse bending and to produce twist through bending/twist coupling. The dimensions and structure of the system are from Crawley and Lazarus (1991): the length is L=292 *mm* along the y axis, width C=152 *mm* along the x axis, and the plate thickness is 0.83 *mm*; 10 of the biomorph actuator pairs are 51x51 *mm* while the other 5 pairs are 25x51 *mm*, all with thickness 0.25 *mm*. The plate is cantilevered along the x axis (boundary condition y=0).

Three characteristic magnitudes are studied: 1) nondimensional longitudinal bending $W_1=M_2/C$; 2) twist in radians $W_2=(M_3-M_1)/C$; and 3) fractional transverse chamber $W_3=[M_2-(M_3-M_1)/2]/C$. M_1 and M_3 are the deflection measurements at the outer transverse edges; M_2 is the plate centerline deflection. C is the width of the plate. The validity of the 2D solution can be seen from Figures 4, where the current 2D solution is compared to experimental data (from Crawley and Lazarus, 1991) and to a 3D solution (Ha, Keilers, and Chang, 1992). The $[0/\pm45]_s$ substrate case is shown with applied voltage field 394 *V*/*mm*; the $[+30_2/0]_s$ substrate case is similar. Figure 5 shows the deflection for the $[0/\pm45]_s$ thin plate, with the vertical scale enlarged. The maximum deflection is 6.20 *mm*. The results calculated from the 2D simplified thin plate model show good agreement with the experimental data and the 3D model. The prediction for W_1 is very close to the data, like the 3D model prediction. W_2 also agrees closely with the data, better than the 3D case. W_3 agrees well initially with the experimental data but both 2D and 3D models diverge from the data far from the clamped edge.

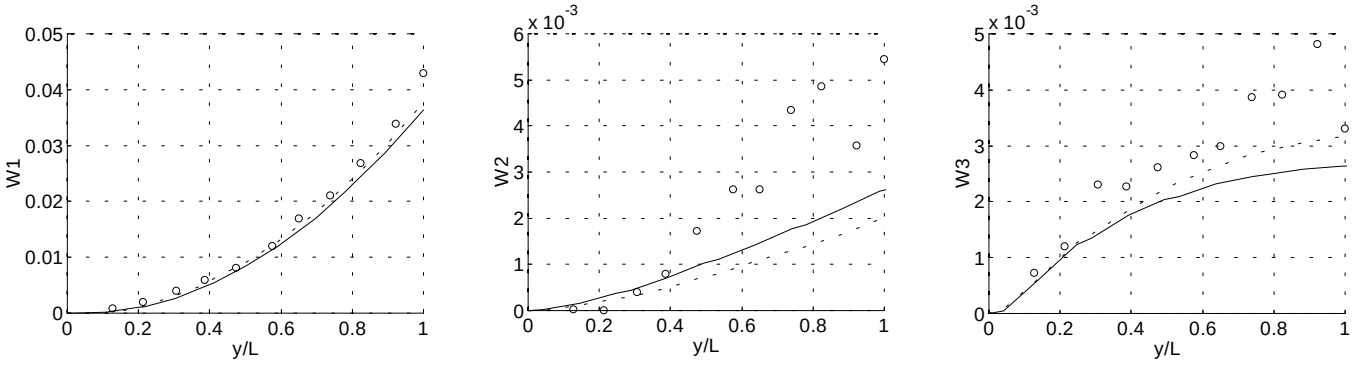

*Figure 4. W_1, W_2, and W_3 Comparisons Between the Present 2D Solution (*solid*), a 3D Solution (*dashed*), and Experimental Data (*circles*)*

Figure 5. Plate Deflection for Figure 4 Example

Computational efficiency is greatly increased via the 2D model. Such efficiency will be a key factor for real-time vibration control and optimal design of large piezoelectric sensor/actuator structures. Table 1 compares the element size (and overall problem size in parentheses) in terms of number of nodes, number of mechanical and electrical degrees-of-freedom (*Mdof* and *Edof*, respectively), and the size of the stiffness matrix *K*.

Table 1. 2D and 3D Model Comparison for Element Size (and for Problem Size)

Model	*Nodes*	*Mdof*	*Edof*	*K Order*
2D DKQ	*4(187)*	*12(561)*	*1(15)*	*12(561)*
3D (Ha, 1992)	*8(374)*	*24(1122)*	*4(374)*	*32(1496)*

OPTIMAL SHAPE CONTROL

The deflection of a composite plate is a function of the geometry and material properties of the piezoelectric actuators, the applied voltage, and the layout and number of the piezoelectric actuators on the plate. This section presents three different optimal shape control solutions: determination of optimal input actuator voltages, determination of the optimal layout of actuators on the plate, and determination of optimal number of actuators, all to obtain a prescribed deflection shape. These optimization procedures employ the model and FEM solution developed previously.

Applied Voltage Optimization

Let the number of actuators p be less than the number of nodes m where deflections W are to be controlled. In the general case the desired deflections W_d cannot be satisfied exactly and the error vector is $e=W-W_d$. The map between the vector V of input voltages and the vector W of output deflections is linear given the actuator layout:

$$W = W_{Tr} + W_T + CV \tag{26}$$

where W_{Tr} is the deflection due to the surface traction, W_T is the thermal deflection, and column vectors C_j of matrix C are the output nodal deflections when a unit voltage is applied to the j^{th} actuator with all other voltages zero. The nodal deflections W are expressed by defining a selecting matrix S for the nodal variables q (using Equation (23)):

$$W = Sq = SK^{-1}F_{Tr} + SK^{-1}F_T + SK^{-1}L^eP_{ae}V \tag{27}$$

and so the terms for Equation (26) are:

$$W_{Tr} = SK^{-1}F_{Tr} \qquad W_T = SK^{-1}F_T \qquad C = SK^{-1}L^eP_{ae} \tag{28}$$

where K is the global FEM stiffness matrix, F_{Tr} and F_T are the surface traction and thermal forces, P_{ae} is the matrix which maps the voltages of elements to the voltages of actuators, $V^e = P_{ae}V$, and:

$$L^e = \begin{bmatrix} (P_1^e)^T L_1^e & (P_2^e)^T L_2^e & \cdots & (P_{n_e}^e)^T L_{n_e}^e \end{bmatrix} \tag{29}$$

where P_i^e are the columns of the matrix P^e which relates the contribution of the element stiffness matrices to the global stiffness matrix. L_i^e is given in Tong (1997).

For applied voltage shape optimization, a quadratic cost function $f(W(V))=e^TQe$ must be minimized, where e is the deflection error $W-W_d$ and Q is a positive-definite diagonal weighting matrix. The constraints are the governing equations and boundary conditions (Equation (16) and one set from Equations (17-20), simplified as discussed earlier). Since nodal deflections W have been solved in terms of input voltages V, the equality constraints are merged into the expression of the cost function $f(W(V))$. The upper and lower bounds of the p actuator voltages, $\overline{V}$ and $\underline{V}$, can be expressed as $2p$ linear inequality constraints on V. These constraints can be written in matrix form as $kV-R\leq 0$ where k is a $2p\times p$ matrix and R is a vector of actuator voltage bounds. The applied voltage shape optimization problem is stated as:

Minimize: $f(V)=(W-W_d)^T Q(W-W_d)$
Subject to: $kV-R\leq 0$

For V^* to be a local optimum for this problem, Kuhn-Tucker multipliers (Minoux, 1986) $\lambda\geq 0$ exist such that:

$$\nabla f(V^*)+\lambda^T\nabla(kV^*-R)=\mathbf{0} \qquad \lambda_i(kV-R)_i=0 \qquad i=1,2,\cdots,2p \tag{30}$$

where λ is a $2p\times 1$ vector and ∇ is the gradient. We must solve:

$$2C^TQCV^*+k^T\lambda=2C^TQ(W_d-W_{Tr}-W_T) \tag{31}$$

for V^*, subject to constraints $\lambda\geq\mathbf{0}$ and $\lambda_i(kV^*-R)_i=0$, where i indicates the i^{th} element of λ and (kV^*-R), not a Kronecker summation.

Since Q is a positive-definite diagonal matrix, the cost function $f(V)$ is strictly convex. The search space of the input voltages V is a strictly convex set. Hence, the solution of this optimization problem is a global minimum and it must be unique.

Actuator Location Optimization

More generally, the location of the actuators on the plate may also be determined to control shape. The actuators are best placed in the regions of high average strain and away from strain nodes (areas of zero strain, Crawley and de Luis, 1987). Finding an optimal layout of the actuators using continuous coordinates is very complicated. Therefore, possible actuator locations will be preassigned through a vector α of binary variables whose elements α_i are 1 to indicate the presence and 0 the absence of an actuator. In this case, deflection W is a function of α through the matrix C:

$$C(\alpha) = SK^{-1}(\alpha)L(\alpha) \tag{32}$$

$$K(\alpha) = K_s + \left[\overline{K}_1 P_{pe}\alpha \quad \overline{K}_2 P_{pe}\alpha \quad \cdots \quad \overline{K}_{n_q} P_{pe}\alpha\right] \tag{33}$$

$$K_s = \sum_{i=1}^{n_e} (P_i^e)^T K_{s\,i}^e P_i^e \qquad\qquad L(\alpha) = L^e Diag(P_{pe}\alpha) P_{ae} \tag{34}$$

where the subscript s indicates the plate global stiffness matrix K composed of substrate material only, $\overline{K}_i$ is a matrix formed by i (from 1 to n_e) columns of the transformed element stiffness matrices, $(P_i^e)^T (K_{a\,i}^e - K_{s\,i}^e) P_i^e$. P_{pe} is a matrix like P_{ae}, mapping the possible locations to the element, L^e is given in Equation (29), and $Diag(P_{pe}\alpha)$ is a diagonal matrix whose elements are the intermediate layout variables.

The actuator location shape optimization problem is written as a quadratic, nonlinear, integer mixed mathematical programming problem:

Minimize: $f(V,\alpha) = (W(\alpha) - W_d)^T Q (W(\alpha) - W_d)$

Subject to: $kV - R \le 0$ $\qquad$ $\alpha_i = 0$ or 1 $\qquad$ $\sum_{i=1}^{n_p} \alpha_i = p$

where n_p is the number of possible preassigned locations.

The existence of the solution of this optimization problem under a given layout, $\alpha \sim V^*$, is also given by the Kuhn-Tucker necessary condition and again Equation (31) must be solved. The α solution searching

is an outer loop optimization problem. When the $\alpha \sim V^*$ solution is obtained both the layout of actuators and the voltages applied on the actuators are optimal.

This optimization problem is highly nonlinear. The solution methods depend on the number of actuator pairs, their possible locations, and the constraints. Certain integer mixed optimization programming (such as the Branch-and-Bound technique) may be used to reduce the feasible solution space.

Number of Actuators Optimization

By changing the constraint $\sum_{i=1}^{n_p} \alpha_i = p$ in the actuator location shape optimization problem to $\underline{p} \le \sum_{i=1}^{n_p} \alpha_i \le \overline{p}$ where $\overline{p}$ and $\underline{p}$ are the upper and lower bounds for p, the number of actuators shape optimization problem results. The problem of the optimal number of actuators becomes a new outer loop and the $\alpha \sim V^*$ solution searching will be more complicated.

Optimization Results

A Matlab computer code OPSC (optimal shape control) has been developed to implement the three types of shape optimization discussed above. For solution algorithm details and a flow chart see Tong (1997). Two numerical examples are presented in this section, one for the applied voltage shape optimization problem and the other for the actuator location shape optimization problem.

Applied Voltage Shape Optimization Example

The actuator/plate system for this example was presented by Ha, Keilers, and Chang (1992). The substrate material is T300/976 composite with a stacking sequence of $[0/\pm 45°]_s$. The fifteen biomorph piezoelectric actuators are PZT G1195N, surface bonded. Two edges of the plate are simply supported with y=0 pinned and y=372 on rollers while the remaining edges are free. The length is L=372 *mm* along the y axis, width C=228 *mm* along the x axis, and the plate thickness is 0.75 *mm*; all biomorph actuator pairs are 60x60 *mm* with thickness 0.13 *mm*. The plate was exposed to a temperature increase of 50°F (relative to the

zero strain temperature) on the top and a drop of 50°F on the bottom. Only the steady-state case of thermal equilibrium is considered. The maximum transverse displacement is 1.70 mm which occurs at the plate center under the given conditions. The desired deflection is zero at all nodes.

The optimal input voltages and resulting deformation of the plate were determined by the OPSC. The characteristic nondimensional deflections W_1, W_2, and W_3 are shown in Figure 6. For comparison, the results of applying uniform input voltage to all actuators are also shown in this figure.

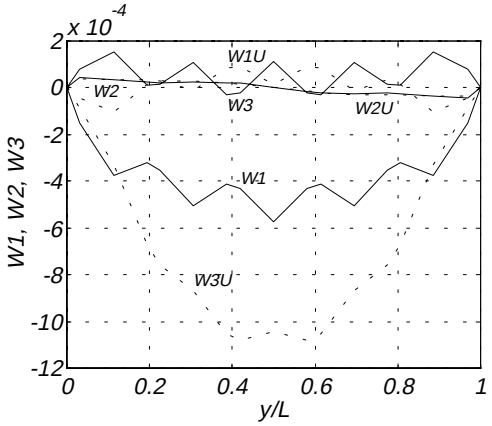

*Figure 6. W_1, W_2, and W_3 for Optimal (*solid*) and Uniform (*dashed*) Voltages*

In Figure 6, W_{iU} represents the uniform voltage results, while W_i are the optimal voltage results. The uniform input voltage case sacrifices the fractional transverse chamber W_{3U} and controls the longitudinal bending W_{1U}. But with applied voltage optimization the control of W_3 has to be tightened instead of W_1 since W_3 is more significant than W_1. Also, the maximum nondimensional deflection W_1 of the optimal case is roughly 50% of W_{3U} in the uniform voltage case. The uniform voltage case causes large deflections along the two free edges of the plate. W_{2U} and W_2 are small and close to each other.

Figure 7a (left) shows the deflection condition for the thin plate under thermal loading with no actuation. Figure 7b (right) shows the same thin plate under optimal voltage shape control. The vertical scales are enlarged.

Figure 7. Optimal Voltage Example Deflections

More actuator pairs are desirable to achieve the target shape. But a large number of actuators is neither practical nor economical. Therefore, the second example presents actuator location optimization.

Actuator Location Shape Optimization Example

This example solves for the optimal layout of the specified total nine actuators (p=9) to minimize thermal deformation of a laminated composite thin plate. The system has the same dimensions, materials and thermal environment as the previous example, but with two differences: 1) the actuators are surface embedded instead of surface bonded; and 2) the four corners are simply supported (one pinned at the origin and the other three on rollers). The fifteen possible preassigned actuator locations are from the previous example, n_p=15. Again, the desired deflection is zero at all nodes.

Voltage constraints (ignored in the first example) are important. Before solving this nine-actuator layout problem, the fifteen optimal input voltages from the first example are checked for infeasible voltages. The results are given in Table 2, whose entries are arranged in the same manner as the actuators on the plate.

Table 2. Optimal Input Voltages (Electric Fields) for 15 Actuators without Voltage Constraints V (V/mm)

85.0 (656.9)	*–36.2 (–278.5)*	*29.7 (228.5)*	*–5.2 (–40.0)*	*50.7 (390.0)*
140.0 (1076.9)	*59.3 (456.2)*	*113.7 (874.6)*	*59.3 (456.2)*	*140.0 (1076.9)*
50.7 (390.0)	*–5.2 (–40.0)*	*29.7 (228.5)*	*–36.2 (–278.5)*	*85.0 (656.9)*

The maximum fields (1076.9 V/mm) reach 90% of the 1200 V/mm coercive field at which the G1195 piezoelectric will depolarize. The actuator location optimization solution with no voltage constraints for the nine actuator problem are given in Table 3. Three out of nine exceed the coercive limit.

Table 3. Optimal Layout and Input Voltages (and Electric Fields) for 9 Actuators without Voltage Constraints V(V/mm)

53.4 (411.8)	-------	*–55.1 (–423.8)*	-------	*56.5 (434.6)*
223.2 (1716.9)	-------	*243.2 (1870.8)*	-------	*232.3 (1786.9)*
53.9 (414.6)	-------	-------	*–73.9 (–568.5)*	*75.0 (576.9)*

Therefore, the optimal layout and input voltages solution is repeated with voltage constraint $V_i \leq 120$ (V) which is 76.9% of the coercive field for each piezoelectric actuator. The results are given in Table 4. Only one actuator location has changed but the voltages are different (six inputs reach the maximum 120 *V*).

Table 4. Optimal Layout and Input Voltages (and Electric Fields) for 9 Actuators with Voltage Constraints V(V/mm)

120.0 (924.0)	-------	*–14.7 (–113.2)*	-------	*104.5 (804.6)*
120.0 (924.0)	-------	*120.0 (924.0)*	*120.0 (924.0)*	*120.0 (924.0)*
120.0 (924.0)	-------	-------	-------	*91.8 (706.9)*

Like Table 2, the entries of Tables 3 and 4 are arranged in the same manner as the actuator pairs on the plate. Figure 8a (left) shows the deflection condition for the thin plate under thermal loading with no actuation. Figure 8b (right) shows the same thin plate with optimal actuator layout and optimal voltage shape control. Again, The vertical scales are enlarged.

Now the actuator layout design and the determination of optimal input voltages are both improved when compared to the first example above because the quadratic cost function value is lower. Table 5

shows the maximum positive and negative transverse displacements (W_{MAX} and W_{MIN}) and the cost function e^TQe value for each case in the two examples.

Figure 8. Optimal Actuator Layout Example Deflections

Table 5. Applied Voltage (V) and Cost Function e^TQe Values (mm^2) for the Optimization Examples

Optimization Example	W_{MAX}*(mm)*	W_{MIN} *(mm)*	e^TQe *(mm^2)*
Example 1 No actuation	1.70	0	162.20
Table 2	0.07	-0.13	0.46
Example 2 No actuation	6.25	0	3100.00
Table 4	0.65	-0.73	18.10

For both optimization examples presented (optimal input voltages of Table 2 and optimal layout and input voltages of Table 4), the maximum transverse displacements and the cost function values are dramatically improved compared to the non-actuated cases. The Table 3 results are not given in Table 5 since that case (unconstrained input voltages) was infeasible. Again, the desired deflection W is zero at all nodes. For all examples in this article (including Figures 4 and 5) the thin plates are discretized into 160 DKQ FEM elements (10 along x and 16 along y); this corresponds to 187 nodes (17 times 11) where the deflection W is controlled.

The number of actuators optimization can also be performed by OPSC, taking the inactivated actuators as extra layers of laminae of different material.

CONCLUSION

Analytical models, FEM solution, and shape optimization was presented for a thin composite plate with piezoelectric actuators surface embedded or bonded in a bimorph arrangement. The 2D DKQ FEM formulation is accurate in predicting deformation and more efficient and simpler than existing 3D models. Three optimal shape control problems have been formulated and solved, the applied voltage, actuator layout, and actuator number shape optimizations. The applied voltage problem requires linear mathematical programming but the actuator layout and number problems require integer-mixed highly non-linear mathematical programming. Two numerical examples were presented, for the first two optimization problems. A novel method using a vector of binary variables is introduced for the second two problems. These optimization techniques may be used for both optimal design (actuator layout and actuator number optimization) and for on-line optimal shape control (applied voltage). A Matlab computer code OPSC has been developed for designing large-scale laminated structures containing distributed piezoelectric actuator biomorph units. Compared to previous research work with 3D models, it was found that the efficiency and the simplicity of the 2D DKQ FEM model was critical for solving large-scale shape design and optimization problems. The present methods may readily be extended to dynamics and vibration analyses for the actuator/plate system.

REFERENCES

S.K. Agrawal, D. Tong, and K. Nagaraja, 1994, "Modeling and Shape Control of Piezoelectric Actuator Embedded Elastic Plates," *J Intel Mat Syst and Structures*, 5(4): 514-521.

L.R. Calcote, 1969, *The Analysis of Laminated Composite Structures*, Van Nostrand Reinhold.

E.F. Crawley and K.B. Lazarus, 1991, "Induced Strain Actuation of Isotropic and Anisotropic Plates," *AIAA Journal*, 29(6): 944-951.

E.F. Crawley and J. de Luis, 1987, "Use of Piezoelectric Actuators as Elements of Intelligent Structures," *AIAA Journal*, 25(10): 1373-1385.

P. Donthireddy and K. Chandrashekhara, 1996, "Modeling and Shape Control of Composite Beams with Embedded Piezoelectric Actuators", Composite Structures, 35(2): 237-244.

J.L. Fanson and T.K. Caughey, 1987, "Positive Position Feedback Control for Large Space Structures," AIAA Paper 87-0902.

M.V. Gandhi and B.S. Thompson, 1992, *Smart Materials and Structures*, Chapman and Hall, London.

K. Ghosh and R.C. Batra, 1995, "Shape Control of Plates using Piezoceramic Elements", AIAA Journal, 33(7): 1354-1357.

S.K. Ha, C. Keilers, and F.K. Chang, 1992, "Finite Element Analysis of Composite Structures Containing Distributed Piezoceramic Sensors and Actuators," *AIAA Journal*, 30(3): 772-780.

T.J.R. Hughes, 1987, *The finite Element Method: Linear Static and Dynamic Finite Element Analysis*, Prentice-Hall.

J. Jia and C.A. Rogers, 1989, "Formulation of a Laminated Shell theory Incorporating Embedded Distributed Actuators," *Adaptive Structures*, ed. B. K. Wada, ASME, pp.25-34.

C.K. Lee and F. Moon, 1990, "Modal Sensors and Actuators," *Journal of Applied Mechanics*, 57: 434-441.

M. Minoux, 1986, *Mathematical Programming: Theory and Algorithms*, Wiley.

A.E. Sepulveda and L.A. Schmit, 1991, "Optimal Placement of Actuators and Sensors in Control-Augmented Structural Optimization," *Intl J Num Meth Engr*, 32: 1165-1187.

D. Tong, 1997, "Modeling and Optimal Shape Control of a Laminated Composite Thin Plate with Piezoelectric Actuators Surface Embedded or Bonded", MS Thesis, Ohio University.

A.C. Ugrual, 1981, *Stresses in Plates and Shells*, McGraw-Hill.